Research Article

대한치과재료학회지 53(3) : 103-120, 2026
Korean Journal of Dental Materials (*Korean J Dent Mater*)
ISSN:2384-4434 (Print); 2384-3268 (Online)
Available online at http://www.kadm.org
http://dx.doi.org/10.14815/kjdm.2026.53.3.103

가시광 조사에 의한 TEPA-rGO 코팅 TiO_2 나노튜브의 균종 의존적 항균 효과

문경숙, 배지명, 오승한*

원광대학교 치과대학 치과생체재료학교실 및 생체재료매식연구소

Effects of TEPA-rGO Deposition Time and Visible-Light Irradiation on the Species-Dependent Antibacterial Activity of TiO_2 Nanotube Arrays

Kyoung-Suk Moon, Ji-Myung Bae, Seunghan Oh*

Department of Dental Biomaterials and the Institute of Biomaterials and Implant, Wonkwang University College of Dentistry, Iksan, Republic of Korea

본 연구는 테트라에틸렌펜타민(TEPA)으로 기능화된 환원 그래핀 산화물(rGO)의 증착시간과 470 nm 가시광선 조사가 TiO_2나노튜브의 항균 활성 및 세포 적합성에 미치는 영향을 평가하였다. 전기영동 증착법으로 1분 또는 3분 동안 코팅한 시편에 470 nm 파장의 빛을 조사하여 녹농균(*Pseudomonas aeruginosa*)과 황색포도상구균(*Staphylococcus aureus*)에 대해 집락형성능 시험 및 항산화 효소 분석으로 항균 활성을 평가하였고, 인간 중간엽 줄기세포(hMSCs)에 대해서는 MTT 분석을 통해 세포 생존율, 즉 세포적합성을 평가하였다. 모든 결과변수는 표면처리와 광조사를 고정인자로 하는 이원 분산분석(two-way ANOVA)으로 분석하였으며, 상호작용이 유의한 경우에는 단순주효과(simple effects) 분석을 추가로 시행하였다. Kubelka-Munk Tauc 분석 결과 밴드갭은 3.21-3.31 eV로 나타나 밴드갭 감소는 관찰되지 않았고, 확산반사에서 구한 겉보기 흡수율(1-R)만 가시광 영역에서 약간 증가하였다. 녹농균에서는 표면처리와 광조사가 상호작용 없이 독립적인 가산효과를 나타냈으며, 3분 코팅과 광조사를 병합한 군은 광조사하지 않은 대조군 대비 집락형성능 수를 60.2% 감소시켰다. 반면 황색포도상구균에서는 두 인자 간 상호작용이 유의하였고, 3분 코팅은 광조사 없이도 집락형성능 수를 46.6% 감소시켰으며 광조사에 의한 추가 감소는 없었다. MTT 분석 결과 코팅은 줄기세포 생존율에 영향을 주지 않았고 광조사는 48시간에 생존율을 소폭 낮추었으나, 모든 실험군의 생존율은 70% 이상으로 본 시험조건에서 세포독성은 관찰되지 않았다. 이러한 결과는 TEPA-rGO가 가시광선 감응보다는 접촉 매개 항균 반응과 부합하며, 광 구동 요소는 코팅되지 않은 TiO_2나노튜브 기질 자체와 관련되어 있을 가능성을 시사한다.

색인단어 : 테트라에틸렌펜타민(TEPA), 환원 그래핀 산화물(rGO), 이산화타이타늄 나노튜브, 가시광선, 항균효과

Kyoung-Suk Moon (ORCID: 0000-0001-6534-3045)
Ji-Myung Bae (ORCID: 0000-0002-8607-8604)

*Correspondence: Seunghan Oh (ORCID: 0000-0002-7250-721X)
460 Iksan-Daero, Iksan, Jeonbuk 54538, Republic of Korea
Affiliation: Department of Dental Biomaterials and Institute of Biomaterials - Implant, Wonkwang University College of Dentistry, Iksan, Jeonbuk, Republic of Korea
Tel: +82-63-850-6982, Fax: +82-63-857-6982
E-mail: shoh@wku.ac.kr

Received: Aug. 13, 2026; Revised: Sep. 04, 2026; Accepted: Sep. 07, 2026

Introduction

Implant-associated infections remain one of the most challenging complications in orthopedic, dental, and other biomedical implant applications (1-3). Despite advances in surgical techniques and sterilization protocols, postoperative infections persist at rates of approximately 0.5–3% in primary implants and are considerably higher in revision surgeries (4). These infections are driven by the rapid colonization of the implant surface by pathogenic bacteria. Once adhered, the bacteria form biofilms that shield them from host immune responses and markedly reduce antibiotic efficacy, often necessitating complex revision surgery (5-8). Therefore, infection and biofilm formation are critical barriers to the long-term success of implantable medical devices.

Titanium and its alloys are among the most widely used implant materials because of their mechanical strength, corrosion resistance, and biocompatibility (9, 10). However, the bioinert nature of bare titanium surfaces limits early osseointegration and provides no intrinsic antibacterial property, leaving the surface susceptible to microbial adhesion (2, 11). Among the surface modifications developed to address this issue, titanium dioxide nanotube arrays (TiO_2 NTs) fabricated by electrochemical anodization offer a high-surface-area nanostructure that promotes osteoblast adhesion, enhances protein adsorption, and permits controlled delivery of drugs or biomolecules (12-15). TiO_2 is also photocatalytic under ultraviolet irradiation, generating reactive oxygen species (ROS) that damage microbial membranes and intracellular components (16, 17). Anatase TiO_2, however, has a wide band gap of approximately 3.2 eV, restricting band-to-band activation to ultraviolet light, which is clinically impractical because of its low tissue penetration, phototoxicity, and limited ambient fraction (18, 19).

The integration of reduced graphene oxide (rGO) with TiO_2 nanostructures has been widely proposed to address this limitation (20, 21). rGO extends light absorption into the visible region by acting as a photosensitizer, facilitating charge-carrier separation and electron transport (22, 23), and exhibiting intrinsic antibacterial properties and good cytocompatibility (24, 25). Although rGO/TiO_2 composites have been produced via hydrothermal synthesis, chemical vapor deposition, and sol-gel routes (26, 27), these approaches are time-consuming, require high temperatures, or yield poor uniformity. Electrophoretic deposition (EPD) is a facile low-temperature alternative, and the amine functionalization of rGO with tetraethylenepentamine (TEPA) imparts the positive surface charge needed to stabilize aqueous dispersions and enable uniform cathodic deposition.

The wavelength used here, 470 nm, was selected for three reasons. It lies immediately below the anatase absorption edge (approximately 3.2 eV, 385 nm), so that any photoresponse must arise from sub-band-gap rather than band-to-band transitions, which makes this wavelength informative for distinguishing a substrate-derived from a coating-derived contribution. Blue light in the 400–470 nm range is already delivered intraorally by dental light-curing units and by blue-light antimicrobial devices, so the irradiation condition is clinically accessible. Finally, tissue penetration and phototoxicity are more favorable than for ultraviolet light (18, 19). Longer wavelengths, including the 600–700 nm region in which the coated and uncoated surfaces differed most in absorbance, were not selected because that difference reflects the broad, non-selective optical absorption of the graphene-based layer rather than a defined semiconductor transition, and because 1.8–2.1 eV photons are further removed from any plausible activation threshold; that region nevertheless merits examination in future work.

A previous study from our group examined TiO_2 NTs coated with nonfunctionalized and aminated rGO and reported antibacterial activity under visible light (33). The present work uses the same deposition platform but addresses a different question. The earlier report compared terminal functional groups at a single deposition condition, whereas the present study varied the deposition time (1 versus 3

min) and 470 nm irradiation as two crossed factors so that their main effects and interaction could be separated, re-evaluated the band gap after Kubelka-Munk transformation of the diffuse reflectance data as recommended for scattering samples (30), and compared the response of a gram-negative with that of a gram-positive species. Because several deposition times had already been screened in that earlier work, the present study is positioned as a follow-up that isolates deposition time and irradiation as experimental factors rather than as the first report of a new material. The present study was nevertheless conducted separately from that work: all specimens were newly fabricated and all optical and biological data reported here were acquired independently for this study, and no measurement, figure, or numerical value overlaps with the previous report.

Therefore, the purpose of this study was to determine how TEPA-rGO deposition time and 470 nm irradiation jointly influence the optical properties, morphology, and antibacterial efficacy of TiO_2 NT arrays against *Staphylococcus aureus* and *Pseudomonas aeruginosa*, and their cytocompatibility with human mesenchymal stem cells (hMSCs), with all quantitative outcomes analyzed by two-way analysis of variance (ANOVA) using surface treatment and irradiation as fixed factors.

Materials and Methods

1. Preparation of TEPA–rGO/TiO_2 NTs

TiO_2 NTs (diameter, 100 nm) were prepared by anodizing pure titanium sheet (99.5%, 250 μm thick; Hyundai Titanium Co., Incheon, Korea) at 20 V for 30 min in 0.5% hydrofluoric acid (w/v; Merck Co., Chicago, IL, USA) and annealing at 450 °C for 2 h (28). The TEPA-functionalized rGO (Sigma-Aldrich Co., St. Louis, MO, USA) was dispersed in deionized water (0.5 mg/mL) with magnesium nitrate hexahydrate (0.05 mg/mL; Sigma-Aldrich) via ultrasonication (VC 505; Sonics & Materials Inc., Newtown, CT, USA). EPD at a direct current of 50 V for 1 or 3 min, using a platinum counter electrode positioned 2 cm from the substrate, resulted in the generation of TEPA-1 and TEPA-3 groups (29). The specimens were washed and dried at 60 °C for 24 h. Uncoated NTs (NT) served as the control, and enzyme activity and hMSCs viability assays compared NT with TEPA-1 alone.

2. Characterization of TEPA–rGO/TiO_2 NTs

Diffuse reflectance spectra were obtained at 300–1000 nm using an integrating-sphere spectrophotometer (SolidSpec-3700; Shimadzu Co., Kyoto, Japan), with a barium sulfate white plate as the 100% reflectance reference and the blocked beam as the 0% baseline. One specimen per group was scanned once, as is customary for diffuse reflectance measurement of this type; the reported values are therefore single determinations rather than means. As reflectance rather than transmittance was measured, the instrument output (absorbance A) was converted to reflectance ($R = 10^{-A}$) and then to the Kubelka-Munk function, $F(R) = (1 - R)^2/2R$, which is proportional to the absorption coefficient for an optically thick, diffusely scattering layer. The band gap (Eg) was obtained from the Tauc plot.

$$(F(R) \cdot h\nu)^{1/n} = B(h\nu - Eg) \quad (1)$$

where $h\nu = 1239.841/\lambda$ is the photon energy in eV, B a constant, and n = 2 for the indirect gaps of anatase TiO_2 and rGO (30). A least-squares line fitted to the linear portion of the absorption edge—the interval of maximum slope with a coefficient of determination above 0.999, falling between 3.59 and 3.76 eV—was extrapolated to the photon-energy axis to obtain Eg. The quantity (1 - R) at 470 nm, and its mean over 400–700 nm, was computed as an apparent absorbed fraction. Because this quantity derives from diffuse reflectance alone, it comprises all light that was not reflected, including light lost to scattering, to transmission into the

substrate, and to non-productive absorption by the carbon layer; it therefore quantifies neither visible-light harvesting nor photocatalytically available absorption. The top and cross-sectional morphologies were examined using field-emission scanning electron microscopy (FE-SEM; S-4800, Hitachi Co., Tokyo, Japan).

3. Visible light irradiation

A laboratory-fabricated 470 nm light-emitting diode (LED) strip mounted on an aluminum support served as a visible light source. Each specimen was placed in a culture plate 4 cm below the strip and irradiated at 60 mW/cm² for 15 min for all in vitro tests, corresponding to a delivered dose of approximately 54 J/cm². Specimen and medium temperatures were not recorded during irradiation; the possible contribution of photothermal heating is therefore considered in the Discussion and listed among the study limitations.

4. Cell viability assay

hMSCs obtained commercially from Lonza Co. (Basel, Switzerland) were used. Cells were cultured in α-modified Eagle's minimum essential medium (Invitrogen Co., Carlsbad, CA, USA) supplemented with 10% fetal bovine serum (Invitrogen) and 1% antibiotics (Invitrogen). For the live/dead assay, hMSCs were seeded on specimens in a 24-well plate (1×10^4 cells/well). After 24 h, the specimens were irradiated for 15 min. Following an additional 24 or 48 h, 500 μL of phosphate-buffered saline (PBS, Invitrogen) containing 2 μM calcein acetoxymethyl ester (Invitrogen) and 4 μM ethidium homodimer-1 (Invitrogen) was added. After 30 min, live (green) and dead (red) cells were observed using an inverted fluorescence microscope (CKX41; Olympus Co., Tokyo, Japan).

Metabolic activity was measured using a 3-(4,5-dimethylthiazol-2-yl)-2,5-diphenyltetrazolium bromide (MTT) Assay Kit (Sigma-Aldrich). The culture and irradiation conditions matched those used in the live/dead assay. At 24 and 48 h, 100 μg/mL MTT solution was added, and specimens were incubated at 37 °C with 5% CO_2 for 4 h. Dimethyl sulfoxide (Sigma-Aldrich) was added to dissolve the formazan crystals, and absorbance was read at 570 nm on a microplate reader (n = 3/group). The data are expressed as percent viability relative to the non-irradiated NT control.

5. Antibacterial assay

S. aureus (ATCC 25923, Manassas, VA, USA) and *P. aeruginosa* (PA14) (31) were incubated in fresh media for 24 h. Bacterial suspension (500 μL) was adjusted to 1×10^5 colony-forming units (CFU)/mL and inoculated on the specimens (1×1 cm²). After another 24 h, the irradiated groups were exposed to a 470 nm LED for 15 min. Bacteria on each specimen were collected, diluted in 100 μL of PBS, plated on agar plates (100 mm diameter), and incubated at 37 °C. Colonies were counted after 24 h and expressed as viable counts ($\times 10^4$ CFU/mL). Each group comprised five specimens that were inoculated, irradiated, and processed separately, and one specimen constituted one independent statistical unit (n = 5 per group).

6. Enzyme activity assay

Superoxide dismutase (SOD) and catalase (CAT) activities were measured to evaluate oxidative stress induced by irradiation. Enzyme extraction was performed as previously described (32). The cultivation and irradiation conditions matched those used in the antibacterial assay. Bacteria were collected and centrifuged (5,000 rpm, 10 min), washed with PBS, and sonicated (VCX-130, Sonics & Materials Inc.) for 20 s (5 s pulses at 3 s intervals). The supernatant was collected by further centrifugation at 12,000 rpm for 20 min at 4 °C. The lysates were assayed for SOD (EIASODC kit, Invitrogen) and CAT (CAT 100 Kit, Sigma-Aldrich) at 450 and 570 nm, respectively, according to the manufacturer's protocols. Protein concentration was determined using the Bradford Reagent (Sigma-Aldrich), and enzyme activities were

normalized to total protein (U/mg protein). Because of the limited bacterial yield from a single specimen, bacteria recovered from two separately inoculated specimens were pooled to form one sample; eight specimens per group therefore yielded four samples, and one pooled sample constituted one independent statistical unit (n = 4 per group). Pooling was performed only within an experimental group and never across groups.

7. Statistical analyses

Data are expressed as the mean ± standard deviation. Each outcome was analyzed by two-way ANOVA with surface treatment and 470 nm irradiation as fixed factors, including the interaction term. Viable counts were analyzed in a 3 × 2 design (surface: NT, TEPA-1, TEPA-3; irradiation) with n = 5 per cell, enzyme data in a 2 × 2 design (NT, TEPA-1) with n = 4 per cell, and MTT data in a 2 × 2 design with n = 3 per cell. Because colony counts are count data, their distribution was examined before analysis; the normality of the model residuals and the homogeneity of the cell variances were satisfied for both species (*P. aeruginosa*, Shapiro-Wilk W = 0.990, p = 0.993 and Levene F = 1.17, p = 0.352; *S. aureus*, W = 0.976, p = 0.726 and F = 0.50, p = 0.774), so untransformed counts were analyzed. An analysis of $\log_{10}$-transformed counts was performed as a sensitivity check and reproduced the same pattern of significance (*P. aeruginosa*: surface $p < 0.001$, irradiation $p < 0.001$, interaction p = 0.388; *S. aureus*: surface $p < 0.001$, irradiation p = 0.341, interaction p = 0.002). Where the interaction was significant, the main effects were not interpreted in isolation; instead, simple effects were tested against the pooled error term, namely the effect of irradiation within each surface and the effect of surface within each irradiation condition, and the three within-surface tests were additionally checked with the Holm correction. For *P. aeruginosa* SOD, Levene's test indicated heterogeneity of variance (p = 0.025), and the analysis was therefore repeated with a heteroscedasticity-robust test, which led to the same conclusions (p = 0.017). For *S. aureus* SOD, the residuals deviated from normality (p = 0.011) because of one low value in the irradiated TEPA-1 group; the non-parametric Kruskal-Wallis test likewise indicated no significant difference among groups (p = 0.063), so the conclusion is unchanged. Pairwise comparisons among cell means were performed using Tukey's multiple comparisons test. In the figures, groups not sharing a lowercase letter differ significantly, and individual data points are overlaid on the bars. Statistical significance was set at $p < 0.05$. All analyses were performed using GraphPad Prism (version 8.4.3; GraphPad Software, San Diego, CA, USA). The two-way ANOVA results for all outcomes are presented in Table 1, and the simple-effects analyses for the two outcomes with a significant interaction in Table 2.

Results

1. Optical properties and morphology

All the groups exhibited a steep anatase absorption edge near 385 nm (Figure 1A). Below the absorption edge, NT showed the highest absorbance, which decreased with deposition time. In the visible region the order reversed: the apparent absorbed fraction (1-R) at 470 nm increased from 87.6% (NT) to 88.8% (TEPA-1) and 89.4% (TEPA-3), and its mean over 400–700 nm from 89.5% to 91.0%. The largest difference between the coated and uncoated surfaces occurred in the broad 600–700 nm feature (Figure 1A), consistent with the non-selective optical absorption of a graphene-based layer. Extrapolation of the $(F(R)h\nu)^{1/2}$ edge yielded band gaps of 3.26 eV (NT), 3.31 eV (TEPA-1), and 3.21 eV (TEPA-3) ($R^2 > 0.999$; Figure 1B), all within the anatase range, so the coating did not narrow the fundamental gap. It should be emphasized that (1-R) is an apparent absorbed fraction obtained from diffuse reflectance: it indicates that little of the incident 470 nm light was reflected, but it does not establish that the corresponding energy was available to drive a photocatalytic reaction. Because the

values were obtained from a single spectrum per group, they are reported without an estimate of measurement variability.

FE-SEM revealed that NTs consist of a well-ordered tubular array with clean, open pores, whereas both coated groups showed wrinkled sheet-like layers progressively covering the openings with increasing deposition time, with the NT architecture preserved beneath the coating (Figure 2). The thickness, mass, and areal coverage of the deposited layer and its chemical composition were not quantified in the present study, so the difference between TEPA-1 and TEPA-3 is described in morphological terms only (see Limitations).

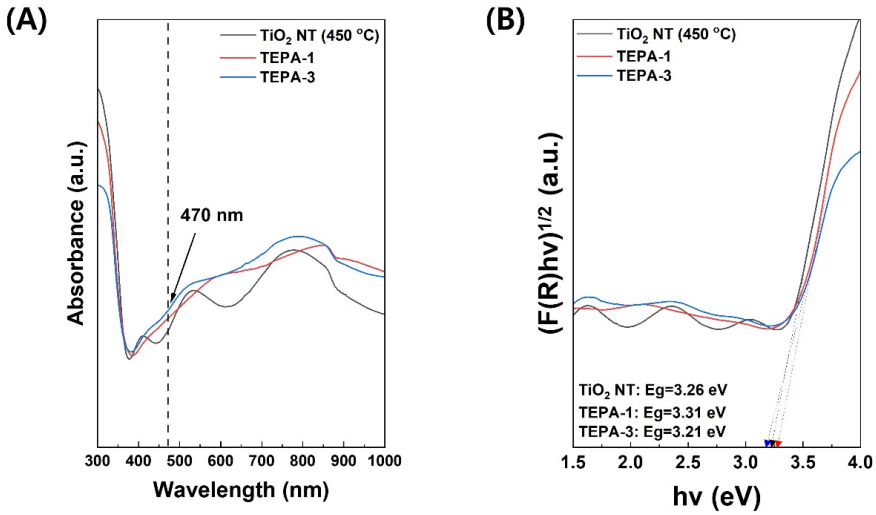


Figure 1. Optical characterization of the uncoated (NT), TEPA-rGO-decorated TiO_2 nanotube arrays deposited via EPD over 1 min (TEPA-1), and 3 min (TEPA-3) surfaces. (A) Diffuse reflectance absorbance spectra over 300–1000 nm; the dashed line marks the 470 nm activation wavelength. (B) Tauc plots of the Kubelka-Munk-transformed spectra, $(F(R)h\nu)^{1/2}$ versus $h\nu$; dashed lines indicate linear extrapolation of the absorption edge to the photon-energy axis and arrowheads mark the resulting band gaps.

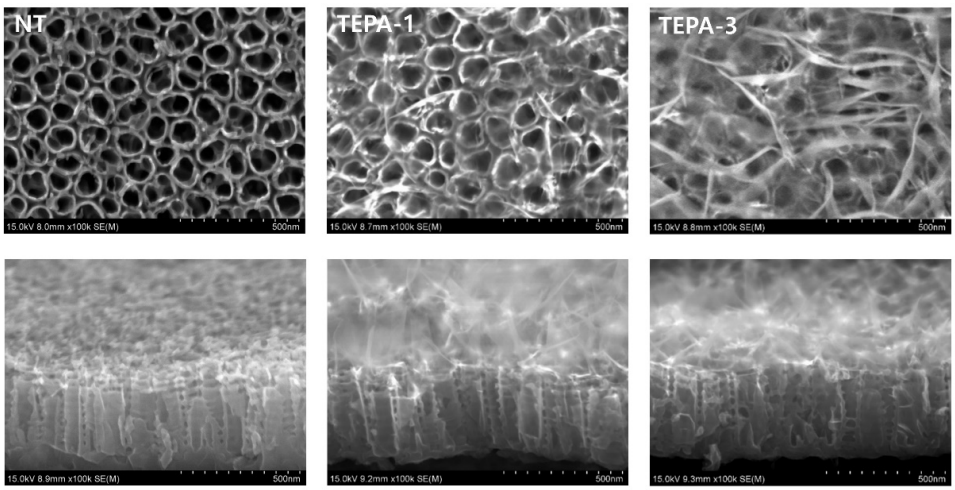


Figure 2. Field-emission scanning electron micrographs of the uncoated (NT), TEPA-rGO-decorated TiO_2 nanotube arrays deposited via EPD over 1 min (TEPA-1), and 3 min (TEPA-3) surfaces. Upper row, top views; lower row, cross-sectional views. The uncoated array shows clean, open nanotube orifices, whereas in the coated arrays wrinkled sheet-like layers progressively cover the openings with increasing deposition time. The tubular architecture is preserved beneath the coating in all three groups (scale bar = 500 nm).

2. Antibacterial performance

The viable counts are presented in Figure 3 and the two-way ANOVA in Table 1. For *P. aeruginosa*, both surface treatment and irradiation were significant factors ($p < 0.001$), whereas their interaction was not ($p = 0.468$), indicating that the two factors acted independently and additively. Irradiation lowered viable counts on every surface by a comparable proportion (NT, -28.6%, $p < 0.001$; TEPA-1, -41.0%, $p < 0.001$; TEPA-3, -39.4%, $p < 0.001$). Irradiated TEPA-3 carried fewer bacteria than non-irradiated NT ($p <$

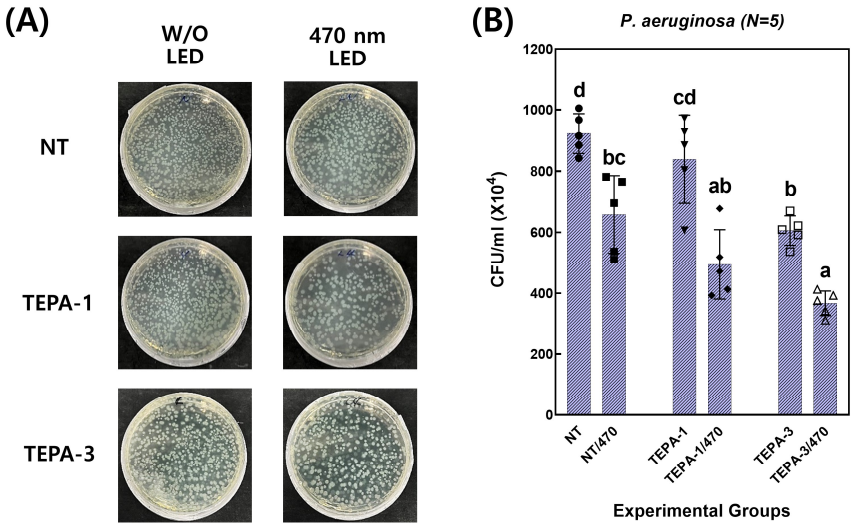


Figure 3. Antibacterial activity against *Pseudomonas aeruginosa*. (A) Representative agar plates corresponding to the uncoated (NT), TEPA-rGO-decorated TiO_2 nanotube arrays deposited via EPD over 1 min (TEPA-1), and 3 min (TEPA-3) surfaces without and with 470 nm irradiation (60 mW/cm^2, 15 min). (B) Viable counts are expressed as $\times 10^4$ colony-forming units per milliliter. Groups not sharing a lowercase letter differ significantly (Tukey's multiple comparisons test; $p < 0.05$).

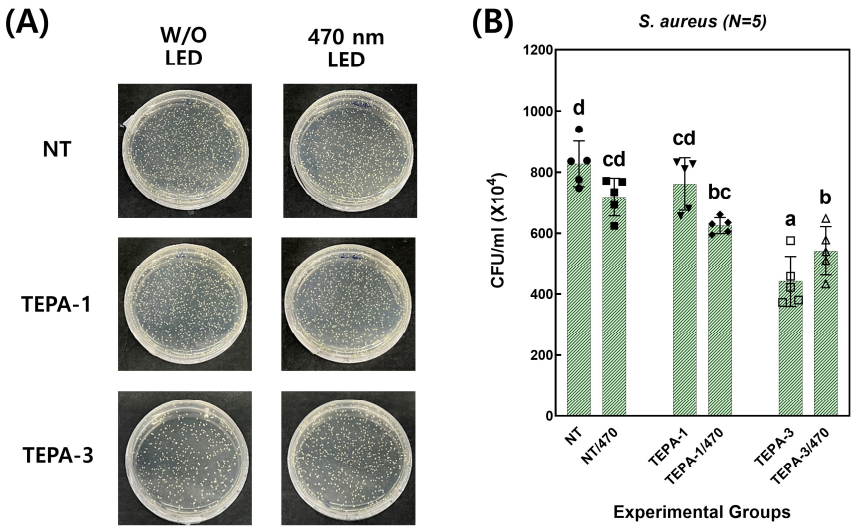


Figure 4. Antibacterial activity against *Staphylococcus aureus*. (A) Representative agar plates corresponding to the uncoated (NT), TEPA-rGO-decorated TiO_2 nanotube arrays deposited via EPD over 1 min (TEPA-1), and 3 min (TEPA-3) surfaces without and with 470 nm irradiation. (B) Viable counts are expressed as $\times 10^4$ colony-forming units per milliliter. Groups not sharing a lowercase letter differ significantly ($p < 0.05$).

0.001), irradiated NT (p = 0.001), and its own dark counterpart (p = 0.009), corresponding to a 60.2% reduction relative to non-irradiated NT (Figure 3).

For *S. aureus*, the surface × irradiation interaction was significant (p = 0.002), so the main effects were not interpreted in isolation (Table 1). In the simple-effects analysis (Table 2), irradiation lowered viable counts on NT (-13.2%, p = 0.023) and on TEPA-1 (-17.9%, p = 0.006), whereas on TEPA-3 the counts were slightly higher under light (+22.6%, p = 0.036); the last comparison was not significant after Tukey adjustment across all six cell means (p = 0.267) and is therefore not regarded as a robust difference. The surface effect was

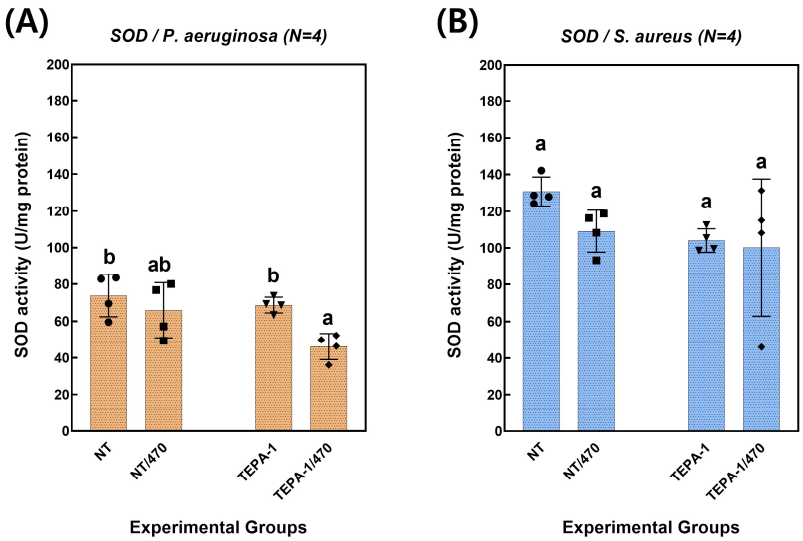


Figure 5. Superoxide dismutase activity in bacteria recovered from the uncoated (NT) and TEPA-rGO-decorated TiO_2 nanotube arrays deposited via EPD over 1 min (TEPA-1) surfaces without and with 470 nm irradiation. (A) *P. aeruginosa*; (B) *S. aureus*. Activities are normalized to total protein. Groups not sharing a lowercase letter differ significantly (p < 0.05).

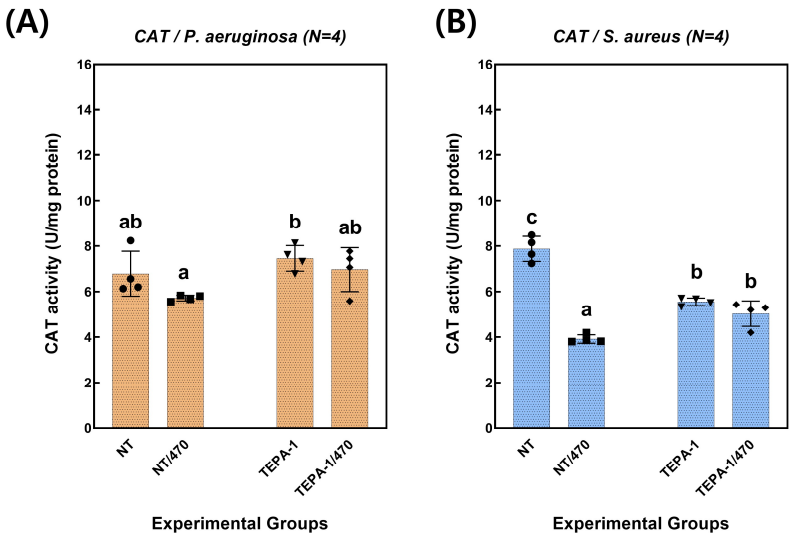


Figure 6. Catalase activity in bacteria recovered from the uncoated (NT) and TEPA-rGO-decorated TiO_2 nanotube arrays deposited via EPD over 1 min (TEPA-1) surfaces without and with 470 nm irradiation. (A) *P. aeruginosa*; (B) *S. aureus*. Activities are normalized to total protein. Groups not sharing a lowercase letter differ significantly (p < 0.05).

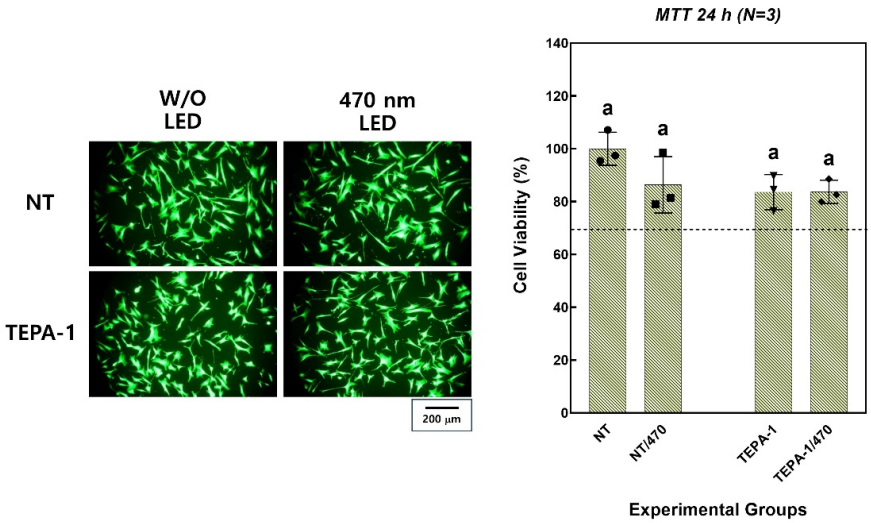


Figure 7. Cytocompatibility of human mesenchymal stem cells on the uncoated (NT) and TEPA-rGO-decorated TiO_2 nanotube arrays deposited via EPD over 1 min (TEPA-1) surfaces without and with 470 nm irradiation after 24 h. Left, calcein acetoxymethyl ester and ethidium homodimer-1 staining, in which live cells fluoresce green and dead cells red (Scale bar = 200 μm). Right, relative viability determined using the tetrazolium reduction assay and expressed as a percentage of the non-irradiated NT control. The dashed line marks the 70% cytotoxicity threshold specified by ISO 10993-5. Groups not sharing a lowercase letter differ significantly ($p < 0.05$). No factor was significant in the two-way ANOVA at 24 h (Table 1).

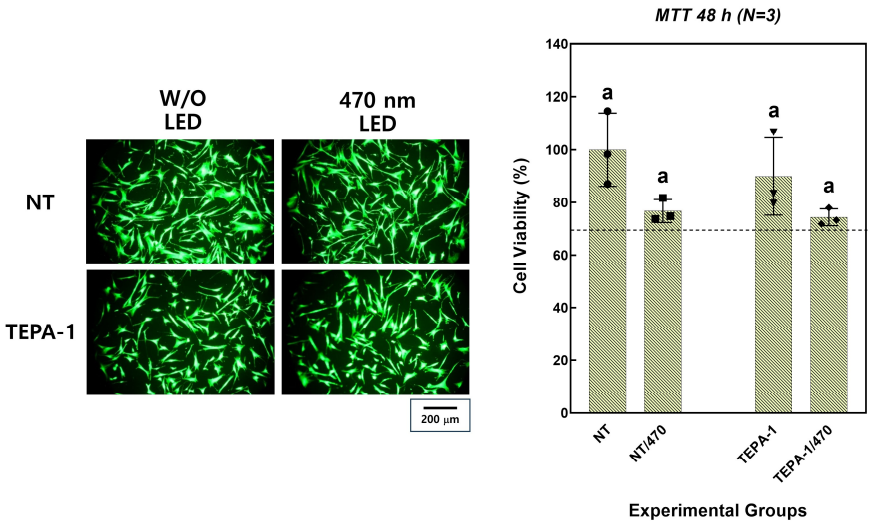


Figure 8. Cytocompatibility of human mesenchymal stem cells on the uncoated (NT) and TEPA-rGO-decorated TiO_2 nanotube arrays deposited via EPD over 1 min (TEPA-1) surfaces without and with 470 nm irradiation after 48 h. Left, calcein acetoxymethyl ester and ethidium homodimer-1 staining (Scale bar = 200μm). Right, relative viability determined using the tetrazolium reduction assay and expressed as a percentage of the non-irradiated NT control. The dashed line marks the 70% threshold specified by ISO 10993-5. Groups not sharing a lowercase letter differ significantly ($p < 0.05$). The main effect of irradiation was significant in the two-way ANOVA ($p = 0.012$; Table 1), although no pairwise comparison among the four groups reached significance after Tukey adjustment.

significant both in the dark ($p < 0.001$) and under irradiation ($p = 0.003$). Non-irradiated TEPA-3 carried fewer colonies than all NT and TEPA-1 groups ($p \leq 0.006$), corresponding to a light-independent 46.6% reduction relative to non-irradiated NT (Figure 4).

3. Bacterial antioxidant enzyme activity

Enzyme assays were used to evaluate light-induced oxidative stress in the NT and TEPA-1 groups. For *P. aeruginosa* SOD, both surface treatment ($p = 0.033$) and irradiation ($p = 0.012$) were significant factors, without interaction. The irradiated TEPA-1 group showed the lowest

Table 1. Two-way analysis of variance of surface treatment and 470 nm irradiation for each outcome

Outcome	Factor	F (df)	*p* value
P. aeruginosa viable count	Surface	24.15 (2, 24)	< 0.001
	Irradiation	61.83 (1, 24)	< 0.001
	Surface × Irradiation	0.78 (2, 24)	0.468
S. aureus viable count	Surface	41.26 (2, 24)	< 0.001
	Irradiation	3.46 (1, 24)	0.075
	Surface × Irradiation	8.21 (2, 24)	0.002
P. aeruginosa SOD	Surface	5.82 (1, 12)	0.033
	Irradiation	8.79 (1, 12)	0.012
	Surface × Irradiation	2.01 (1, 12)	0.182
S. aureus SOD	Surface	3.13 (1, 12)	0.102
	Irradiation	1.59 (1, 12)	0.232
	Surface × Irradiation	0.77 (1, 12)	0.397
P. aeruginosa CAT	Surface	6.61 (1, 12)	0.024
	Irradiation	4.32 (1, 12)	0.060
	Surface × Irradiation	0.59 (1, 12)	0.458
S. aureus CAT	Surface	8.65 (1, 12)	0.012
	Irradiation	118.40 (1, 12)	< 0.001
	Surface × Irradiation	69.77 (1, 12)	< 0.001
Cell viability, 24 h	Surface	5.05 (1, 8)	0.055
	Irradiation	2.54 (1, 8)	0.150
	Surface × Irradiation	2.61 (1, 8)	0.145
Cell viability, 48 h	Surface	1.07 (1, 8)	0.332
	Irradiation	10.31 (1, 8)	0.012
	Surface × Irradiation	0.41 (1, 8)	0.540

The table reports the F ratio (degrees of freedom in parentheses) and *p* value of the two main effects and their interaction, obtained by two-way ANOVA for each outcome. The surface factor had three levels (NT, TEPA-1, and TEPA-3) for viable counts and two levels (NT and TEPA-1) for all other outcomes. Pairwise comparisons among cell means were performed with Tukey's multiple comparisons test and are shown in Figure 3–8; simple-effects analyses for the outcomes with a significant interaction are given in Table 2. df, degrees of freedom; SOD, superoxide dismutase; CAT, catalase

activity, differing significantly from non-irradiated NT (p = 0.012) and from its dark counterpart (p = 0.040). No significant effect was observed in *S. aureus* (all $p \geq 0.102$; Kruskal-Wallis p = 0.063) (Figure 5). SOD and CAT activities are indirect markers of oxidative stress and do not constitute direct measurement of reactive oxygen species.

For *P. aeruginosa* CAT, only the surface effect was significant (p = 0.024). For *S. aureus*, the surface × irradiation interaction was significant (p < 0.001), and the simple-effects analysis showed that irradiation suppressed CAT activity on the uncoated surface (-50.3%, p < 0.001) but not on TEPA-1 (-9.4%, p = 0.099); activity on TEPA-1 was already lower than on NT in the dark (p < 0.001) and was higher than on NT under irradiation (p = 0.002) (Table 2, Figure 6).

4. Cell viability

Live/dead staining showed predominantly live cells on both NT and TEPA-1 surfaces at 24 and 48 h, regardless of irradiation (Figure 7 and 8). At 24 h, no factor was significant (surface, p = 0.055; irradiation, p = 0.150; interaction, p = 0.145). At 48 h, only the irradiation effect was significant (p = 0.012), with no surface effect (p = 0.332) or interaction (p = 0.540): metabolic activity was 76.7% on irradiated NT and 74.4% on irradiated TEPA-1, relative to the non-irradiated NT control, whereas non-irradiated TEPA-1 retained 89.9%. None of the pairwise comparisons among the four cell means remained significant after Tukey adjustment ($p \geq 0.067$), so the irradiation effect is evident only as a main effect. All groups remained above the 70% viability threshold specified by ISO 10993-5, indicating that no cytotoxicity was detectable under the present test conditions.

Discussion

Kubelka-Munk analysis showed that the band gap remained at 3.21–3.31 eV irrespective of coating, indicating that the 2.64 eV photons delivered at 470 nm are unlikely to drive band-to-band excitation. Little of the incident light was reflected from any surface, and irradiation reduced *P. aeruginosa* survival on all of them, including the uncoated array. One plausible interpretation

Table 2. Simple-effects analysis for the two outcomes with a significant surface × irradiation interaction

Outcome	Simple effect	Test statistic (df)	p value
S. aureus viable count	Irradiation within NT	t (24) = -2.42	0.023
	Irradiation within TEPA-1	t (24) = -3.02	0.006
	Irradiation within TEPA-3	t (24) = 2.22	0.036
	Surface within dark	F (2, 24) = 41.81	< 0.001
	Surface within 470 nm	F (2, 24) = 7.67	0.003
S. aureus CAT	Irradiation within NT	t (12) = -13.60	< 0.001
	Irradiation within TEPA-1	t (12) = -1.79	0.099
	Surface within dark	F (1, 12) = 63.83	< 0.001
	Surface within 470 nm	F (1, 12) = 14.65	0.002

Simple effects were tested against the pooled error term of the corresponding two-way ANOVA. Negative t values indicate a decrease under 470 nm irradiation relative to the dark condition. For the three within-surface tests on *S. aureus* viable counts, the Holm-adjusted p values were 0.047 (NT), 0.018 (TEPA-1), and 0.047 (TEPA-3); the TEPA-3 comparison was not significant after Tukey adjustment across all six cell means (p = 0.267). CAT, catalase; df, degrees of freedom

is that the light-driven component may be associated with sub-band-gap absorption by defect states such as oxygen vacancies and Ti^{3+} centers, which are frequently reported for anodized and annealed TiO_2. On this reading the effect would be associated mainly with the NT substrate rather than with sensitization by the coating. Because such states were not characterized here, and because neither reactive oxygen species nor membrane damage was measured directly, this assignment remains tentative; other sub-band-gap pathways, including states introduced at the rGO/TiO_2 interface, cannot be excluded. The statistical structure was at least consistent with this interpretation, in that coating and irradiation acted as additive main effects without interaction and the light-driven reductions were of similar magnitude on all three surfaces. This pattern is compatible with a photoactive component residing mainly in the substrate, while the coating acted through a separate route of membrane disruption and oxidative stress mediated by rGO (24).

Suppression of *P. aeruginosa* SOD by both factors is consistent with an oxidative-stress response, and its depression by the coating alone suggests a chemical in addition to a photocatalytic source of oxidative stress; because SOD and CAT are indirect markers, however, these data are consistent with, but do not demonstrate, ROS generation. A photothermal contribution cannot be formally excluded, since specimen and medium temperatures were not recorded and the delivered dose (60 mW/cm² for 15 min, approximately 54 J/cm²) is high enough to warrant caution. Two observations nevertheless argue against heating as the dominant mechanism. A photothermal effect would be expected to scale with the optical density of the surface and therefore to be largest on the darkest, thickest coating, whereas the light-driven reduction in *P. aeruginosa* was already present on the uncoated array and did not increase disproportionately with deposition time; and nonspecific thermal damage would not be expected to produce the selective, species-dependent changes in antioxidant enzyme activity that were observed. Direct temperature monitoring is required to settle this point. The *S. aureus* response differed qualitatively, with a significant interaction but no overall irradiation effect. Its thick peptidoglycan attenuates ROS- and contact-mediated damage relative to the gram-negative envelope (19, 24). The 3-min coating reduced colonization in the absence of light but not further under irradiation, which suggests that contact-mediated stress dominates on the thicker layer.

Cytocompatibility testing showed that the TEPA-rGO coating did not affect hMSC viability at either time point, whereas 470 nm irradiation modestly lowered metabolic activity at 48 h on both the uncoated and the coated surface (to 76.7% and 74.4% of the non-irradiated NT control). Because the reduction was of similar size irrespective of coating and no pairwise comparison remained significant after Tukey adjustment, it is more plausibly attributed to the light dose itself than to the coating, and it parallels the light-driven component observed on the uncoated array in the bacterial assays. Viability in all groups nevertheless remained above the ISO 10993-5 threshold, so no cytotoxicity was detectable under the present conditions. An earlier study reported 2.21 and 2.40 eV for aminated and nonfunctionalized rGO (33), but those values were derived from raw absorbance rather than from Kubelka-Munk-transformed data (30); the optical values of the two studies are therefore not directly comparable, and only the biological outcomes can be compared.

TEPA-rGO carries a polyamine chain that provides the colloidal stability and positive surface charge required for uniform cathodic deposition on the TiO_2 NTs. The same chain, however, acts as a bulky spacer between the rGO basal plane and the oxide. Close interfacial contact between rGO and TiO_2 is generally regarded as a prerequisite for the interfacial electronic coupling to which

visible-light sensitization and apparent band-gap narrowing are usually attributed in rGO/TiO_2 composites (20–23). The absence of any narrowing in the present measurements is consistent with the possibility that the TEPA spacer limited this coupling, so that the coating quality achieved by amine functionalization may have been obtained at the expense of electronic communication with the substrate. Because the interface was not characterized directly, this remains an interpretation rather than a demonstrated mechanism. It is nonetheless consistent with the observation that the contact-mediated contribution of the TEPA-rGO layer was more prominent than any visible-light photocatalytic effect that band-gap narrowing would have produced.

The practical value of these findings depends on whether the light dose can be delivered intraorally. The condition used here, 60 mW/cm^2 for 15 min at a working distance of 4 cm, lies within the output range of dental blue-light sources, but continuous 15 min exposure of a defined implant surface is difficult to achieve in the mouth, and the irradiance reaching an implant surface covered by soft tissue would be substantially lower. The most realistic application is therefore not routine irradiation of a functioning implant but decontamination of an exposed implant surface during a procedure, such as open-flap debridement for peri-implantitis or chair-side treatment of a contaminated fixture before placement. In that setting an additive combination of a contact-active surface and a light-triggered component is attractive, because the contact-mediated part continues to act when the light is off. The reductions observed here (46.6–60.2%, well below a 3-log kill) would nevertheless represent an adjunct to mechanical and chemical debridement rather than a replacement for it. The cytocompatibility data are relevant to the same setting: hMSC viability remained above the ISO 10993-5 threshold in all groups and was not affected by the coating, whereas irradiation lowered it modestly at 48 h; this indicates that the surface itself did not compromise the cells responsible for early osseointegration under these in vitro conditions, but that the light dose, rather than the coating, is the parameter that would need to be optimized; osteogenic differentiation and bone formation were not assessed.

Several limitations should be considered. The coating was characterized only by FE-SEM; its thickness, mass, areal coverage, and chemical composition were not quantified, so the difference between TEPA-1 and TEPA-3 is described in morphological terms only. Confirmation by X-ray photoelectron spectroscopy (C 1s and N 1s), Raman D/G band analysis, energy-dispersive spectroscopy mapping, or gravimetric and cross-sectional thickness measurement remains necessary, and the optical measurements were not repeated on independent specimens, so the band gaps are reported without an estimate of measurement variability. Defect states were inferred rather than measured; quantification of Ti^{3+} together with direct detection of reactive oxygen species and of membrane damage would be required to establish the proposed mechanism, and the SOD and CAT data are indirect markers of oxidative stress. TEPA-3, which produced the largest antibacterial effect against *S. aureus*, was not included in the enzyme or hMSC assays, so its oxidative-stress response and cytocompatibility remain unverified and the safety of the thickest coating cannot be concluded. Specimen and medium temperatures were not monitored during irradiation. The number of independent replicates was small (n = 3–5). Finally, only planktonic and early-adherent bacteria were examined; the assay does not model a mature biofilm, and the results should not be extrapolated to anti-biofilm efficacy. In vivo verification remains a task for future research. Within these limits, the main outcome was that coating TiO_2 NTs with TEPA-rGO did not narrow the band gap yet reduced *P. aeruginosa* by 60.2% under 470 nm irradiation while hMSC viability remained above the ISO 10993-5 threshold, an effect that appears to combine a

contact-mediated antibacterial response of the coating with a light-driven component retained by the NT substrate.

Conclusion

In summary, TEPA-rGO was deposited on TiO_2 NTs via electrophoretic deposition, and the coated surfaces differed morphologically with deposition time. Kubelka-Munk analysis showed that the optical band gap remained at 3.21–3.31 eV regardless of coating; instead of narrowing the gap, the coating raised the mean apparent absorbed fraction over 400–700 nm from 89.5% to 91.0%. Coating and 470 nm irradiation acted additively on *P. aeruginosa* with no interaction, the combination reducing viable counts by 60.2% and lowering SOD activity. In *S. aureus*, a significant surface × irradiation interaction indicated that the thicker coating acted largely independently of light (46.6% reduction in the dark). hMSC viability remained above the ISO 10993-5 threshold in all groups; the coating did not affect viability, whereas irradiation modestly lowered it at 48 h, so no cytotoxicity was detectable under the present conditions. Within the limits of the assays used, these results are consistent with a contact-mediated antibacterial response of the TEPA-rGO layer combined with a light-driven component that may be associated largely with the TiO_2 NT substrate; direct measurement of defect states and of reactive oxygen species is required to confirm this interpretation.

Acknowledgements

This study was supported by Wonkwang University in 2025.

References

1. Darouiche RO. Treatment of infections associated with surgical implants. N Engl J Med. 2004;350(14):1422-9.
2. Kadirvelu L, Sivaramalingam SS, Jothivel D, Chithiraiselvan DD, Karaiyagowder Govindarajan D, et al. A review on antimicrobial strategies in mitigating biofilm-associated infections on medical implants. Curr Res Microb Sci. 2024;6:100231.
3. Ahmadabadi HY, Yu K, Kizhakkedathu JN. Surface modification approaches for prevention of implant associated infections. Colloids Surf B Biointerfaces. 2020;193:111116.
4. Seidelman JL, Mantyh CR, Anderson DJ. Surgical site infection prevention: a review. JAMA. 2023;329(3): 244-52.
5. Sharma S, Mohler J, Mahajan SD, Schwartz SA, Bruggemann L, Aalinkeel R. Microbial biofilm: a review on formation, infection, antibiotic resistance, control measures, and innovative treatment. Microorganisms. 2023;11(6):1614.
6. Omwenga EO, Awuor SO. The bacterial biofilms: formation, impacts, and possible management targets in the healthcare system. Can J Infect Dis Med Microbiol. 2024;2024:1542576.
7. Grari O, Ezrari S, El Yandouzi I, Benaissa E, Ben Lahlou Y, Lahmer M, et al. A comprehensive review on biofilm-associated infections: mechanisms, diagnostic challenges, and innovative therapeutic strategies. Microbe. 2025;8:100436.
8. Zhao A, Sun J, Liu Y. Understanding bacterial biofilms: from definition to treatment strategies. Front Cell Infect Microbiol. 2023;13:1137947.
9. Jiang P, Zhang Y, Hu R, Shi B, Zhang L, Huang Q, et al. Advanced surface engineering of titanium materials for biomedical applications: from static modification to dynamic responsive regulation. Bioact Mater. 2023;27:15-57.

10. Zhou X, Xu D, Geng S, Fan Y, Liu M, Wang Q, et al. Mechanical properties, corrosion behavior and cytotoxicity of Ti-6Al-4V alloy fabricated by laser metal deposition. Mater Charact. 2021;179:111302.
11. Mahmoudi P, Akbarpour MR, Lakeh HB, Jing F, Hadidi MR, Akhavan B. Antibacterial Ti-Cu implants: a critical review on mechanisms of action. Mater Today Bio. 2022;17:100447.
12. Jafari S, Mahyad B, Hashemzadeh H, Janfaza S, Gholikhani T, Tayebi L. Biomedical applications of TiO_2 nanostructures: recent advances. Int J Nanomedicine. 2020;15:3447-70.
13. Brammer KS, Oh S, Cobb CJ, Bjursten LM, van der Heyde H, Jin S. Improved bone-forming functionality on diameter-controlled TiO_2 nanotube surface. Acta Biomater. 2009;5(8):3215-23.
14. Pan C, Liu T, Yang Y, Liu T, Gong Z, Wei Y, et al. Incorporation of Sr^{2+} and Ag nanoparticles into TiO_2 nanotubes to synergistically enhance osteogenic and antibacterial activities for bone repair. Mater Des. 2020;196:109086.
15. Masahashi N, Mori Y, Inoue H. Biocompatible functional surface of titanium-based implant materials. Int Mater Rev. 2025;70(6):465-96.
16. Nagaraj K, Radha S, Deepa CG, Raja K, Umapathy V, Badgujar NP, et al. Photocatalytic advancements and applications of titanium dioxide (TiO_2): progress in biomedical, environmental, and energy sustainability. Next Res. 2025;2(1):100180.
17. Castellote M, Bengtsson N. Principles of TiO_2 photocatalysis. In: Ohama Y, Van Gemert D, editors. Applications of titanium dioxide photocatalysis to construction materials. Dordrecht: Springer Netherlands; 2011. p.5-10.
18. Fujishima A, Rao TN, Tryk DA. Titanium dioxide photocatalysis. J Photochem Photobiol C Photochem Rev. 2000;1(1):1-21.
19. Lazic, V, Niksic, V, Nedeljkovic JM. Application of TiO_2 in Photocatalytic Bacterial Inactivation: Review. Int J Mol Sci. 2025;26:10593.
20. Shaik BB, Katari NK, Raghupathi JK, Jonnalagadda SB, Rana S. Titanium dioxide/graphene-based nanocomposites as photocatalyst for environmental applications: a review. ChemistrySelect. 2024;9:e202403521.
21. Lin CH, Chen WH. Graphene family nanomaterials (GFN)- TiO_2 for the photocatalytic removal of water and air pollutants: synthesis, characterization, and applications. Nanomaterials (Basel). 2021;11(12):3195.
22. Kumar A, Choudhary P, Kumar A, Camargo PHC, Krishnan V. Recent progress in understanding the role of graphene oxide, TiO_2 and graphene oxide–TiO_2 nanocomposites as multidisciplinary photocatalysts in energy and environmental applications. Catal Sci Technol. 2025;15:1702-70.
23. Mohammadi M, Rezaee Roknabadi M, Behdani M, Kompany A. Enhancement of visible and UV light photocatalytic activity of rGO- TiO_2 nanocomposites: the effect of TiO_2/graphene oxide weight ratio. Ceram Int. 2019;45(10):12625-34.
24. Liu S, Zeng TH, Hofmann M, Burcombe E, Wei J, Jiang R, et al. Antibacterial activity of graphite, graphite oxide, graphene oxide, and reduced graphene oxide: membrane and oxidative stress. ACS Nano. 2011;5(9):6971-80.
25. Cheng C, Nie SQ, Li S, Peng H, Yang H, Ma L, et al. Biopolymer functionalized reduced graphene oxide with enhanced biocompatibility via mussel inspired coatings/anchors. J Mater Chem B. 2013;1(3):265-75.
26. Shao L, Quan S, Liu Y, Guo Z, Wang Z. A novel gel-sol strategy to synthesize TiO_2 nanorod combining reduced graphene oxide composites. Mater Lett. 2013;107:307-10.
27. Ibrayev N, Zhumabekov A, Ghyngazov S, Lysenko E. Synthesis and study of the properties of nanocomposite materials TiO_2-GO and TiO_2-rGO. Mater Res Express. 2019;6(12):125036.
28. Fang D, Luo ZP, Huang KL, Lagoudas DC. Effect of heat treatment on morphology, crystalline structure and

photocatalysis properties of TiO_2 nanotubes on Ti substrate and freestanding membrane. Appl Surf Sci. 2011;257:6451-61.

29. Yun JH, Wong RJ, Ng YH, Du A, Amal R. Combined electrophoretic deposition-anodization method to fabricate reduced graphene oxide-TiO_2 nanotube films. RSC Adv. 2012;2(23):8164-71.
30. Makula P, Pacia M, Macyk W. How to correctly determine the band gap energy of modified semiconductor photocatalysts based on UV-Vis spectra. J Phys Chem Lett. 2018;9:6814-7.
31. Rahme LG, Stevens EJ, Wolfort SF, Shao J, Tompkins RG, Ausubel FM. Common virulence factors for bacterial pathogenicity in plants and animals. Science. 1995;268:1899-902.
32. Wang X, Shen Y, Thakur K, Han J, Zhang JG, Hu F, et al. Antibacterial Activity and Mechanism of Ginger Essential Oil against *Escherichia coli* and *Staphylococcus aureus*. Molecules. 2020;25(17):3955.
33. Moon KS, Bae JM, Choi EJ, Oh S. Titania nanotubes with aminated reduced graphene oxide as efficient photocatalysts for antibacterial application under visible light. Sci Rep. 2025;15:6127.

Research Article

Effects of TEPA–rGO Deposition Time and Visible–Light Irradiation on the Species–Dependent Antibacterial Activity of TiO_2 Nanotube Arrays

*Kyoung-Suk Moon, Ji-Myung Bae, Seunghan Oh**

Department of Dental Biomaterials and the Institute of Biomaterials and Implant, Wonkwang University College of Dentistry, Iksan, Republic of Korea

This study evaluated how the electrophoretic deposition time of tetraethylenepentamine (TEPA)-functionalized reduced graphene oxide (rGO) and 470 nm visible-light irradiation affect the antibacterial activity and cytocompatibility of TiO_2 nanotube arrays. Arrays coated for one or three minutes were evaluated under 470 nm irradiation (60 mW/cm2, 15 min) against *Pseudomonas aeruginosa* and *Staphylococcus aureus* by colony counting and antioxidant enzyme assays, and on human mesenchymal stem cells by the 3-(4,5-dimethylthiazol-2-yl)-2,5-diphenyltetrazolium bromide (MTT) assay. Each outcome was analyzed by two-way analysis of variance with surface treatment and irradiation as fixed factors, and simple effects were tested where the interaction was significant. Kubelka-Munk Tauc analysis yielded band gaps of 3.21–3.31 eV, indicating no narrowing, whereas the apparent absorbed fraction derived from diffuse reflectance increased only slightly in the visible region. Coating and irradiation acted as independent, additive effects on *P. aeruginosa*, and the three-minute coating combined with irradiation lowered viable counts by 60.2% relative to the uncoated array in the dark. In *S. aureus* the two factors interacted: the three-minute coating lowered counts by 46.6% in the dark, with no further reduction under light. The coating did not affect stem-cell viability, whereas irradiation modestly lowered it at 48 h; viability remained above 70% in all groups, and no cytotoxicity was observed under the present test conditions. These findings are consistent with a contact-mediated antibacterial response of the TEPA-rGO layer rather than with visible-light sensitization, together with a light-driven component that may be associated with the TiO_2 nanotube substrate itself.

Keywords : Tetraethylenepentamine, Reduced graphene oxide, Titanium dioxide nanotube, Visible light, Antibacterial effect